Computational Fluid Dynamics JOURNAL vol.4. no.2 July 1995 (239–262)

NUMERICAL ANALYSIS OF THREE-DIMENSIONAL TURBULENT STRUCTURE IN OPEN CHANNEL FLOW

Hitoshi SUGIYAMA † Mitsunobu AKIYAMA †
Tamaki MATSUBARA † Masaru HIRATA ‡

Abstract

Numerical simulation has been carried out for the developing turbulent flow in an open channel by using Reynolds stress model, in which the convection and the diffusion terms are replaced from differential equations to algebraic equations by adopting Rodi's approximation. In calculation, since the turbulent structure including free surface is different from the closed duct flow, it is necessary to modify the boundary condition. In this study, two different types of calculation have been carried out; one is the narrow open channel with channel aspect ratio 2 to predict the velocity-dip phenomenon, the other is the wide open channel flow with channel aspect ratio 10 to confirm disappearing the velocity-dip phenomenon. The calculated results are compared with the experimental data to examine the validation of the present method. Moreover, the mechanism of the turbulence-driven secondary flow in open channel flow has been investigated by evaluating the generation terms of streamwise vorticity. As a result of this numerical analysis, the present method predict well quantitatively the characteristic features in open channel flow. And the calculated results suggest that the turbulence-driven secondary flow is generated more actively near the free surface of the side wall than the corner region in open channel flow.

1. INTRODUCTION

The turbulent structure of open channel flow is bound up with the existence of free surface. Therefore, it is clear that the turbulent structure of river flow is largely different from that of closed duct flow. In open channel flow, the most characteristic feature is that the maximum velocity appears not at the free surface, but rather just below it. This phenomenon is called the 'velocity-dip', and it is peculiar to open channel flow with small channel aspect ratio. Therefore, the velocity-dip phenomenon is not observed in wide open channel flow. Adding to this characteristic feature, for narrow open-channel, the spanwise distribution of the bed shear stress increases rapidly with distance from the side wall, and it shows a mild peak before reaching the central axis. Beyond this position, it increases again, and attain a maximum at the central axis. In contrast, for the closed-channel flow, the bed shear stress is a minimum at the central axis. Thus, the spanwise variation of bed shear stress in closed-channel flows is out of phase with that in open-channel flows.

Received on February 8, 1995.
† Department of Mechanical Systems Engineering, Utsunomiya University;
Ishii-cho 2753, Utsunomiya 321, Japan
‡ Department of Mechanical Engineering, Shibaura Institute of Technology;
Fukasaku 307, Oomiya 330, Japan

In earlier experimental analysis of free surface, Rajaratanum and Muralidhar [1] have reported that the secondary flow of the second kind induced by anisotropy turbulence had influence on the spanwise distribution of the bed shear stress. For practical purpose, friction laws for rectangular open-channel flows have been studied intensively by many researchers. For instance, from comparison between shear stress distribution in open channel and closed conduit flows at comparable channel aspect ratio, Knight, Demetriou and Humed [2] have presented empirical formula about the bed friction force. Although these researchers recognized the significant contribution of the secondary flows to friction laws, they were not able to reveal its physical mechanism. Nakagawa, Nezu and Ueda [3] have measured the turbulent structure of two-dimensional open channel flow by making use of hot-film anemometer. They concluded that one noticeable influence on turbulent structure is the damping of the vertical velocity fluctuations by the free surface. Judging from this fact, it is easy to guess that the flow pattern of the secondary motion near the free surface differs from that of the closed duct flow. Because the anisotropy turbulence is generated more actively by the damping of vertical velocity fluctuation near the free surface than corner region in the close duct. Moreover, Nezu and Nakagawa [4] have measured in detail the secondary flow pattern, distributions of Reynolds stresses and shear stress distributions along the bed and side wall in three-dimensional open channel flow by using Laser-Doppler anemometer. These measurement results show that a strong free surface vortex is produced due to high anisotropy of turbulence which is caused by the existence of free surface and this vortex produces a velocity-dip and also restrains the development of the bottom vortex. They have also substantiated that the velocity-dip phenomenon disappeared in wide open channel with an increase of the channel aspect ratio. As a theoretical approach, Einstein and Li [5] first ascribed the origin of the secondary flows in straight channel flows to the gradient of Reynolds stresses on the vorticity equation.

In numerical analysis, Naot and Rodi [6] were the first to predict the flow in open channel with turbulence-driven secondary motion by using algebraic Reynolds stress model. They have presented the free surface boundary condition with increasing turbulent dissipation by taking into account the damping effect of the turbulent energy near the free surface. Nezu and Nakagawa [7] have calculated for the turbulent structure in two-dimensional open channel by using modified $k-\varepsilon$ turbulence model. They introduced the damping factor for the turbulent energy near the free surface without increasing turbulent dissipation rate. They achieved this condition by multiplying the surface value of turbulent energy determined from the zero-gradient condition by damping factor. Consequent upon calculation, they summarized the calculated results coincide with the experimental data which have been intensively obtained since 1975 by their own. Celic and Rodi [8] have also carried out for two-dimensional open channel flow by modified version of the $k-\varepsilon$ turbulence model coupled with simplified algebraic expressions for the transport equations of Reynolds stresses, in which the wall proximity effect are retained. For the turbulent structure in compound open channel flow which are characterized by the large shear layers generated by the difference between main channel flow and flood-plain flow, Naot, Nezu and Nakagawa[9] have presented the calculated results compared with the experimental data of vorticity and axial mean velocity except for the distributions of Reynolds stresses. Although many calculated results have presented for open channel flow as described in the above, numerical results which indicate in detail the difference between the calculated results and the

experimental data about not only streamwise velocity and secondary flow pattern but also the distributions of individual Reynolds stresses are few and far between to our knowledge.

Considering the information about a open channel flow which are summarized in the previous paragraph, the numerical study has been carried out for a fully developed turbulent flow in a open channel flow with channel aspect ratio B/h=2 for the purpose of making the turbulent structure clear. The symbol B and h represent channel width and channel depth, respectively. In parallel with this calculation, the other numerical analysis has been carried out for the turbulent structure in wide open channel with aspect ratio B/h=10 in order to confirm whether the present method predict the disappearance of velocity-dip phenomenon indicated by Nezu and Nakagawa [4], or not. The calculated results are compared extensively with the experimental data measured by Nezu and Nakagawa [4], in which the detailed distributions of Reynolds stresses involved. Besides, the three-dimensional calculation has been performed for a developing turbulent flow in open channel with channel aspect ratio $B/h = 2$ with the aim of clarifying the developing behavior of secondary currents.

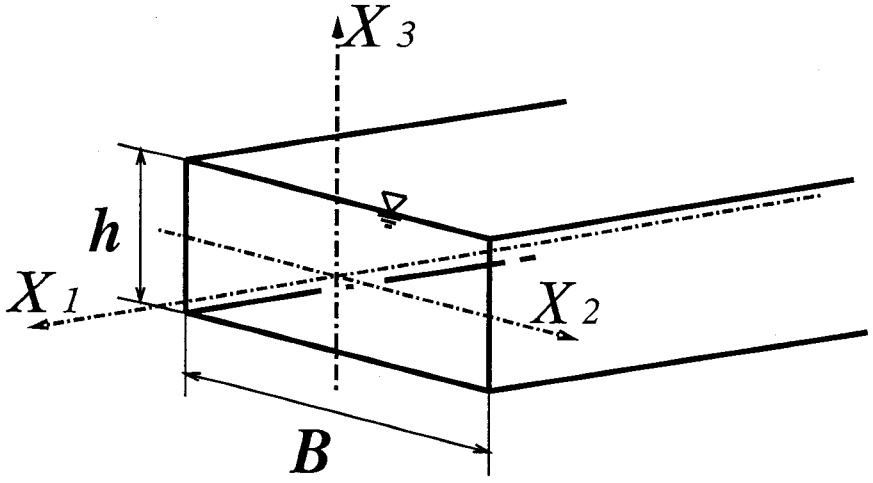

Fig.1: Subject of calculation and coordinate system

2.TECHNIQUE OF ANALYSIS

2.1 Subject of Numerical Analysis

In numerical analysis, the experimental data measured in detail by Nezu and Nakagawa [4] was adopted as a subject of calculation. Figure 1 shows a schematic diagram of the experimental apparatus and the coordinate system set in open channel flow. In Fig.1, X_1, X_2 and X_3 are the coordinate along streamwise velocity, the spanwise direction and the vertical direction to the channel bed, respectively. The free surface corresponds to upper wall of rectangular cross section in Fig.1. The two different types of flow have been carried out in this research; the one is narrow open channel with a width of $B = 20.1$ cm and height of $h = 10.1$ cm, the other is wide open channel with $B = 60.0$ cm and $h = 60.0$ cm. The open channel length is 20 m in both cases.

Reynolds number $Re = U_b 4R/\nu$, where U_b is the bulk mean velocity, R represents hydraulic radius and ν is the kinematic viscosity of water, was set to 9.7×10^4 for narrow open channel and 9.1×10^4 for wide open channel. Measuring cross section locates at 18 m downstream from the entrance of open channel, where the flow corresponds to the fully developed turbulent flow. The experiment has carried out highly accurate measurement in open channel flow by making use of Laser Doppler anemometer.

2.2 Reynolds Stress Model

The anisotropy nature of the turbulence was expressed preciously by the Reynolds stress equations. Nevertheless, an exact analysis of these equations is not yet available so that some modeling effort was required. The set of differential equations governing the transport of the Reynolds stresses is derived from the Navier-Stokes equation as follows:

$$\frac{\mathrm{D}\overline{u_i u_j}}{\mathrm{D}t} = -\left(\overline{u_i u_k}\frac{\partial U_j}{\partial x_k} + \overline{u_j u_k}\frac{\partial U_i}{\partial x_k}\right) + \overline{\frac{p}{\rho}\left(\frac{\partial u_i}{\partial x_j} + \frac{\partial u_j}{\partial x_i}\right)} - \frac{\partial}{\partial x_k}\left[\overline{u_i u_j u_k} - \nu\frac{\partial \overline{u_i u_j}}{\partial x_k} - \overline{\frac{p}{\rho}\left(\delta_{jk}u_i + \delta_{ik}u_j\right)}\right] - 2\nu\overline{\frac{\partial u_i}{\partial x_k}\frac{\partial u_j}{\partial x_k}} \tag{1}$$

The first term of the right hand side is the production term P_{ij}, the second term is the pressure strain correlation π_{ij}, the third term is the diffusion term, and the forth term is the dissipation term ε_{ij}. To get the solution of the Reynolds stress equation in the form presented above is difficult. It is necessary to introduce model assumptions for the correlations appearing in the exact equation. As for the modeling of the convective term and of the diffusion term, the approximation by Rodi [10] was employed. By Rodi's approximation, these terms expressed in a differential form for Reynolds stress component can be transformed into the algebraic equation. In the Reynolds stress model equation, a particularly problematic task is the modeling of the pressure–strain correlation term which is also defined redistribution term. Following Chou [11],the pressure-strain term can be expressed as follows:

$$\overline{\frac{p}{\rho}\frac{\partial u_i}{\partial x_j}} = \frac{1}{4\pi}\int_{\mathrm{vol}}\left\{\overline{\left(\frac{\partial^2 u_l u_m}{\partial x_l \partial x_m}\right)'\frac{\partial u_i}{\partial x_j}} + 2\left(\frac{\partial U_l}{\partial x_m}\right)'\overline{\left(\frac{\partial u_m}{\partial x_l}\right)'\left(\frac{\partial u_i}{\partial x_j}\right)}\right\}\frac{\mathrm{d\,vol}}{|\boldsymbol{x}-\boldsymbol{y}|} + S_{ij} \tag{2}$$

where terms with and without a prime are related to values at $\boldsymbol{y}$ and $\boldsymbol{x}$, respectively and vol represents the volume of subjected space. The first and second term of right hand side of (2) are relevant to the interaction of fluctuating velocities and to that of mean strain and fluctuating velocities, respectively. The term S_{ij} represents the wall effect. In the present model, we adopted the Rotta's linear return-to-isotropy model as the first of the terms $\pi_{ij,1}$ on right of (2). The second term $\pi_{ij,2}$ and the wall effect term $\pi_{ij,w}$ can be expressed as summarized in Table 1. In the modeling of $\pi_{ij,2}$, we made use of the forth-order tensor presented by Launder, Reece and Rodi [12]. The authors [13] described the derivation of these terms in detail.

In Table 1, $f(L/X_w)$ is a function of the dimensionless wall distance. It expresses the influence of the wall and takes the value 1 in its vicinity, approaching 0 in with the increasing distance of it. X_w expresses the distance from the wall and L defined length scale of turbulence. The values of constants have been chosen such that, when $f = 0$, the model yields the correct

Table 1: Modeling of the pressure–strain correlation term

$\pi_{ij,1} + \pi_{ji,1}$	$-c_1 \frac{\varepsilon}{k}\left(\overline{u_i u_j} - \frac{2}{3}k\delta_{ij}\right)$
$\pi_{ij,2} + \pi_{ji,2}$	$-\frac{c_2+8}{11}\left(P_{ij} - \frac{2}{3}P_k\delta_{ij}\right)$ $+\zeta k\left(\frac{\partial U_i}{\partial x_j} + \frac{\partial U_j}{\partial x_i}\right) - \frac{8c_2-2}{11}\left(D_{ij} - \frac{2}{3}P_k\delta_{ij}\right)$
$[\pi_{ij} + \pi_{ji}]_w$	$c_1 = c_1^* + c_1' \cdot f\left(\frac{L}{X_w}\right)$, $c_2 = c_2^* + c_2' \cdot f\left(\frac{L}{X_w}\right)$, $\zeta = \zeta^* + \zeta' \cdot f\left(\frac{L}{X_w}\right)$

$$P_{ij} = -\overline{u_i u_k}\frac{\partial U_j}{\partial x_k} - \overline{u_j u_k}\frac{\partial U_i}{\partial x_k}, \qquad D_{ij} = -\overline{u_i u_k}\frac{\partial U_k}{\partial x_j} - \overline{u_j u_k}\frac{\partial U_k}{\partial x_i}$$

$$P_k = -\overline{u_k u_l}\frac{\partial U_k}{\partial x_l}$$

Table 2: Constants in the pressure–strain correlation term

c_1^*	c_2^*	ζ^*	c_1'	c_2'	ζ'
1.40	0.44	-0.16	-0.35	0.12	-0.10

Reynolds stress components for nearly homogeneous shear flow of Champangne, Harris and Corrsin [14], and, when $f = 1$, the relative magnitude of the stress components agrees with a consensus of near wall turbulence. Moreover, we have used the experimental data of Harris, Graham and Corrsin [15] who reported further homogeneous shear flow data where the strain rate was higher than Champagne, Harris and Corrsin. The constants used in this analysis are summarized in Table 2.

The forth term of (1) is the homogeneous part of dissipation. This term is modeled commonly with the assumption of the isotropic motion for the dissipation, namely:

$$\varepsilon_{ij} = 2\nu\overline{\frac{\partial u_i}{\partial x_k}\frac{\partial u_j}{\partial x_k}} = \frac{2}{3}\delta_{ij}\varepsilon. \tag{3}$$

2.3 Boundary Condition at a Free Surface

The free surface can be considered to a first approximation as a plane of symmetry under the absence of wind-induced shear stress, i.e., a zero gradient is often used as the boundary condition for the velocity components and for the turbulent quantities at the free surface. However, the

presence of a free surface reduces the length scale and, thus, increases the dissipation rate, as pointed out by Hunt [16]. Moreover, since the length scale characterizes the turbulent fluctuation in all three directions, it does not become zero at the surface because the horizontal extent of the eddies is not restricted by the surface. Therefore, it is clear that a zero gradient for turbulent dissipation is not reasonable as a boundary condition at free surface.

Naot and Rodi [17] have presented the following boundary condition for turbulent dissipation on condition that the length scale has a virtual origin with distance y' above the surface and is proportional to the distance from this origin:

$$\varepsilon_s = \frac{c_\mu^{3/4} k^{3/2}}{\kappa} \left(\frac{1}{y'} + \frac{1}{y^*} \right) \tag{4}$$

where subscript s denotes the free surface and $y*$ stands for the distance from the nearest wall. This distance $y*$ included in (4) ensure a smooth transition between the free surface boundary condition and the near wall condition. They adopted y' to be 0.07 times the channel depth h in the calculation. Nezu and Nakagawa [18] suggested a different boundary condition for turbulent energy that has basically the same effect as the turbulent dissipation, i.e., a reduction of turbulent energy near the free surface. They expressed its reduction by multiplying the free surface value k_d of turbulent energy evaluated from the zero–gradient condition by a damping function D as follows:

$$k_s = D\, k_d \tag{5}$$

They recommend the value 0.8 for damping function D following the experimental analysis. On the other hand, Gibson and Rodi[19] have calculated for the two-dimensional open channel flow using a Reynolds stress transport equations with surface effect terms in the pressure-strain correlation. In their calculation, since Reynolds stress equations contain the surface effect term, the boundary conditions at a free surface are the same as those at the symmetry plane of a two-dimensional closed channel. Recently, Naot, Nezu and Rodi [20] have presented the calculation results in compound open channel flow due to the modified length scale at a free surface. Following (4), turbulent dissipation at a free surface shows discontinuous value at the location where the flow depth h varies like a step by the reason why y' is defined as a channel depth h. Considering this fact, they proposed renewal boundary condition for length scale without discontinuity.

As described in the above, it seems that several researchers have proposed the boundary condition at free surface taking account of adjustment with the turbulent model adopted in numerical analysis. In this study, considering the application for compound open channel flow and that the behavior of turbulent near free surface is physically similar to that of wall, the turbulent dissipation ε is defined as following equation:

$$\varepsilon = \frac{c_\mu^{3/4} k^{3/2}}{ky} \tag{6}$$

which is the same expression of wall function. In the above equation, y is the distance between the free surface and first calculated point. The boundary conditions of the other parameters except for ε is equal to that of symmetry plane used in general. As shown in previous paragraph,

the present algebraic Reynolds stress model contains the wall reflection term in pressure-strain correlation, which is also proposed by Gibson and Rodi [19]. This wall reflection term seems to be effective near the free surface.

As mentioned in the introduction, Nakagawa, Nezu and Ueda have investigated the hydraulic behavior near the free surface by making use of hot film anemometer. They have pointed out as the major important result that velocity fluctuation perpendicular to the free surface decreases with approaching the free surface. Its damping effect of velocity fluctuation is similar to that of near the wall. But the damping effect of velocity fluctuation in the vicinity of free surface is stronger than that of near wall, as presented experimentally by Nakagawa et al. As a result of this damping effect, the intensity of velocity fluctuation perpendicular to the free surface displays a small value compared with that of velocity fluctuation near the wall before reaching the free surface. In order to realize the existence of this strong damping effect near the free surface, the value of velocity fluctuation perpendicular to the free surface sets to be zero at not only free surface but also the first grid point from the free surface as a boundary condition. The validity of this treatment have been confirmed from the calculated results with setting zero value at the first grid point and without its condition.

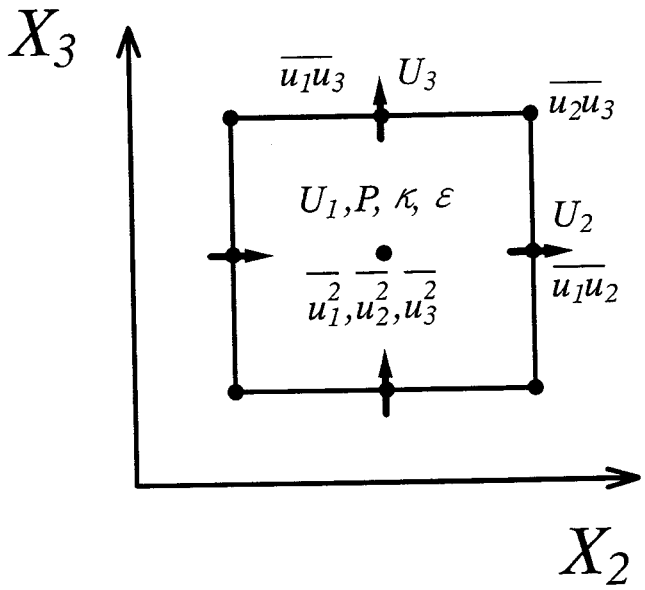

Fig.2: Arrangement of calculation mesh

2.4 Method of Numerical Analysis

A control volume method was adopted with applying the staggered mesh expression for uniform grid points. As a result of using staggered mesh, the locations of Reynolds stresses, vector and scaler parameters on the staggered mesh are located as shown in Fig.2. In order to discretize the convection terms, we employed quadratic interpolation (QUICK) for the momentum equations and power law interpolation (PLDS) for the transport equations of turbulent energy and

turbulent dissipation. The SIMPLE algorithm, which stands for semi-implicit method for pressure linked equation, was used to solve pressure correction and velocity correction. In narrow open channel flow, two kinds of computation has been performed; one is for a fully developed turbulent flow with 30x30 uniform grid points over the half cross section of channel, the other is for developing turbulent flow with 20x20 uniform grid points over the half cross section, 100 grid points along streamwise direction and the Reynolds number is 9.7×10^4 in both cases. In calculation for developing turbulent flow, total length of narrow open channel is 321.6 times the hydraulic radius R of open channel. Hydraulic radius R is defined as the ratio of cross section area to wetted length. In the case of the wide open channel for fully developed flow, 30×92 grids points set over the half cross section and Reynolds number is 9.1×10^4. In regard to grid dependency, it is confirmed that there is not discrepancy between and the calculated results with 30×30 grid points and that with 20×20 grid points for narrow open channel flow.

Calculating for developing turbulent flow, condition of isotropic turbulent flow with constant velocities was used at the inlet. The turbulent energy k and the turbulent dissipation ε are unknown to the experimental data, so that the value of $k = U_b\times10^{-5}$, $\varepsilon = k^{3/2}/4R$ were fixed at the inlet section (U_b denotes the bulk velocity). As for the boundary conditions for k and ε equations, the law of the wall function is useful for calculation on the assumption that both the universal velocity distribution and local equilibrium are realized at the vicinity of the wall.

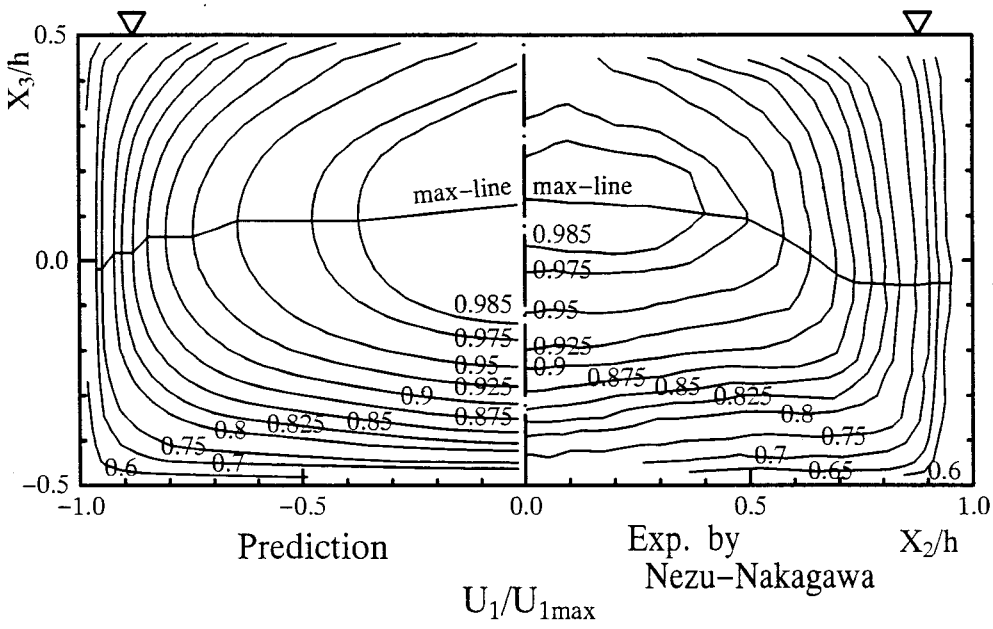

Fig.3: Comparison of streamwise velocity in narrow open channel

3.ANALYSIS RESULTS AND CONSIDERATIONS

3.1 Numerical Analysis in the Case of Channel Aspect Ratio $B/h = 2$

At first, calculated results in narrow open channel are examined. Figure 3 shows the comparison the calculated contour map of streamwise velocity with the experimental data measured by Nezu and Nakagawa [4]. The results of the calculation and the experiments were nondimensionalized by the maximum streamwise velocity U_{1max} in the cross section. Both contour maps are the results for a fully developed turbulent flow region. The max-line in Fig.3 is obtained by plotting points of local maximum streamwise velocity along the vertical line to the X_2 coordinate. The present method predicts well this max-line. Adding to this, the velocity-dip phenomenon, which is peculiar to open channel flow, is observed clearly in both results.

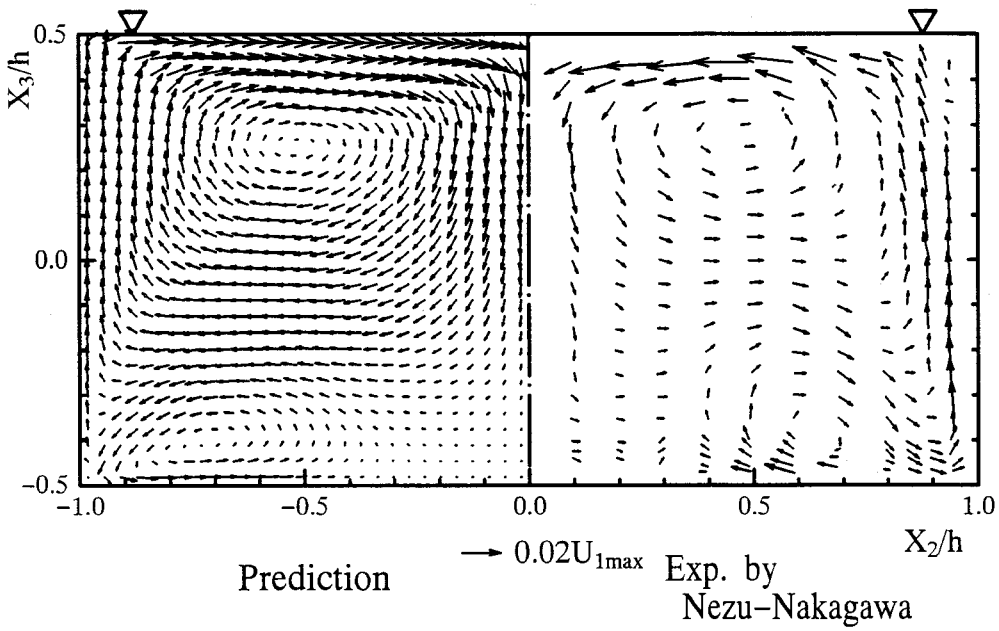

Fig.4: Comparison of secondary currents in narrow open channel

It is clear that this velocity-dip phenomenon is caused by the turbulence-driven secondary motion. Therefore, it is necessary to predict well the secondary currents in order to realize the velocity-dip phenomenon. Figure 4 shows the both results for the velocity vector of secondary flow. In experimental results, a strong vortex occurs near the free surface. This vortex is called the 'free-surface vortex', and its pairing vortex near the bed is called the 'bottom vortex'. The free surface vortex is much stronger than the bottom vortex, and it transports momentum and energy from the side wall toward the channel center near the free surface. The strong downflow that occurs at the channel center causes the velocity-dip as momentum is transported from the free surface toward the mid-depth. The present method can predict well these characteristic features in open channel flow as shown in Fig.4.

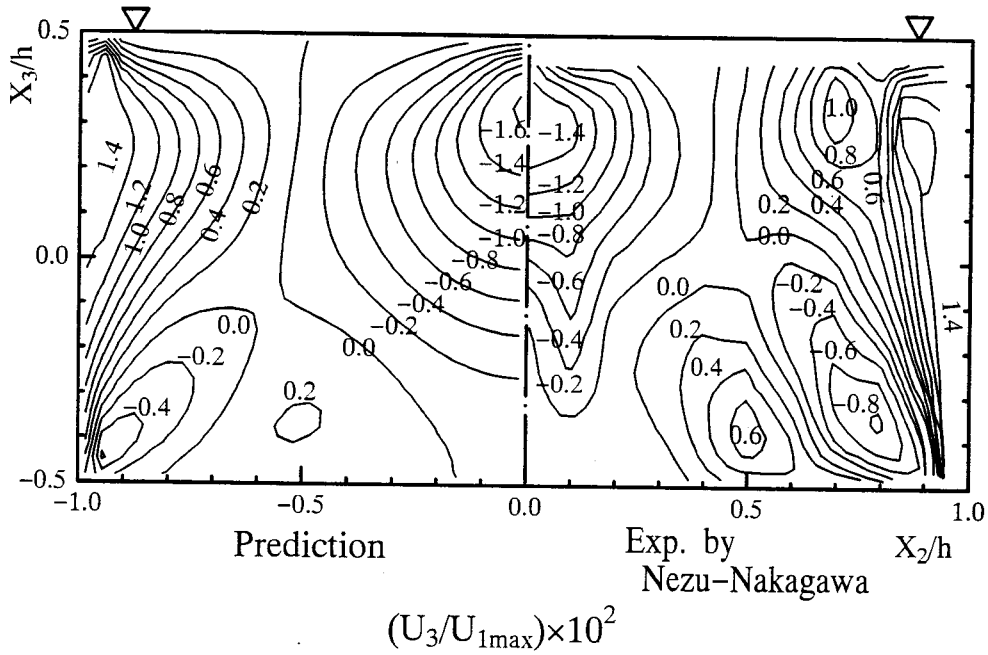

Fig.5: Comparison of vertical velocity in narrow open channel

Figure 5 compares contour maps for vertical velocity U_3. It is found in both results that the maximum absolute value is located near the side wall and the channel center and isoline of zero value proceeds from bed and corner regions toward channel center of the free surface.

Figure 6 shows the comparison of streamline between numerical and experimental results. The definition of streamline is expressed as following form:

$$\psi = \int U_3 \, \mathrm{d}\, x_2 \tag{7}$$

Free-surface vortex and bottom vortex are observed in both results. Free-surface vortex occupies wide region in channel cross section. The present method predicts well the location of these vortex center and value of contours.

In open channel flow, the bed shear stress is different from that of duct flow in its distribution. Figure 7 (a) and (b) show the spanwise distribution of bed shear stress and side wall respectively, which is evaluated from the following equation as well as the experimental results:

$$\frac{U_1}{U_\tau} = 5.75 \log \left(\frac{U_\tau y}{\nu} \right) + 5.5 \tag{8}$$

where y is defined as the distance from the wall. These shear stress distributions are nondimensionalized by mean shear stress of the corresponding wall. For closed-channel flow, it has been reported that the bed shear stress displays the minimum value at the central axis after showing local peaking. But as shown in Fig.7(a), for open-channel flow, the bed shear stress increases rapidly with distance from the side wall, and it shows a mild peak before reaching the central

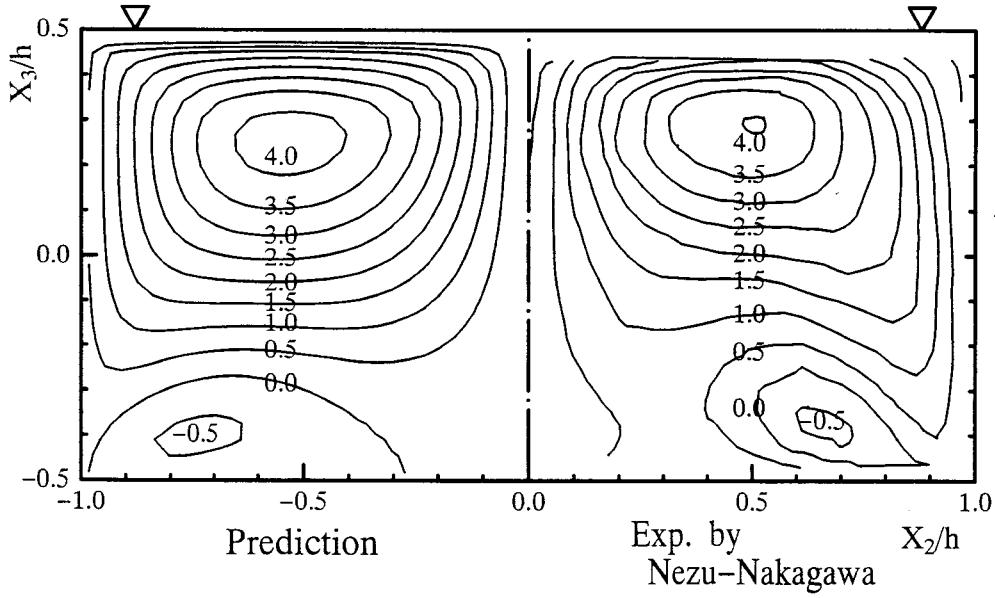

Fig.6: Comparison of streamline in narrow open channel

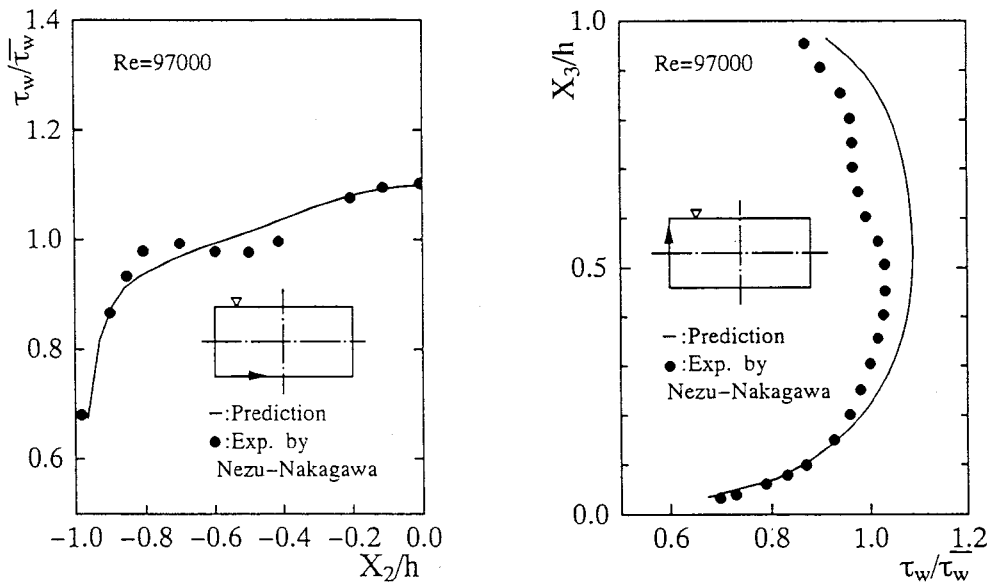

(a) Shear stress along bed (b) Shear stress along side wall

Fig.7: Comparison of wall shear stress in narrow open channel

axis. Beyond this position, it increases again, and attains a maximum value at the central axis. This bed shear stress distribution is also considered as the characteristic feature as well as the velocity-dip phenomenon, which is generated by the downward secondary currents along the central axis and bottom vortex. The maximum value of the central axis is produced as a result of secondary currents transport high level momentum near the free surface to the bed of open channel. Although agreement with the experimental data is not perfect in all detail, the main feature is reproduced by the present method. In regard to the shear stress of side wall, it increases with distance from the bed and decreases gradually toward the free surface after showing maximum value as shown in Fig.7(b). The calculation displays relatively good agreement with the data of experiment.

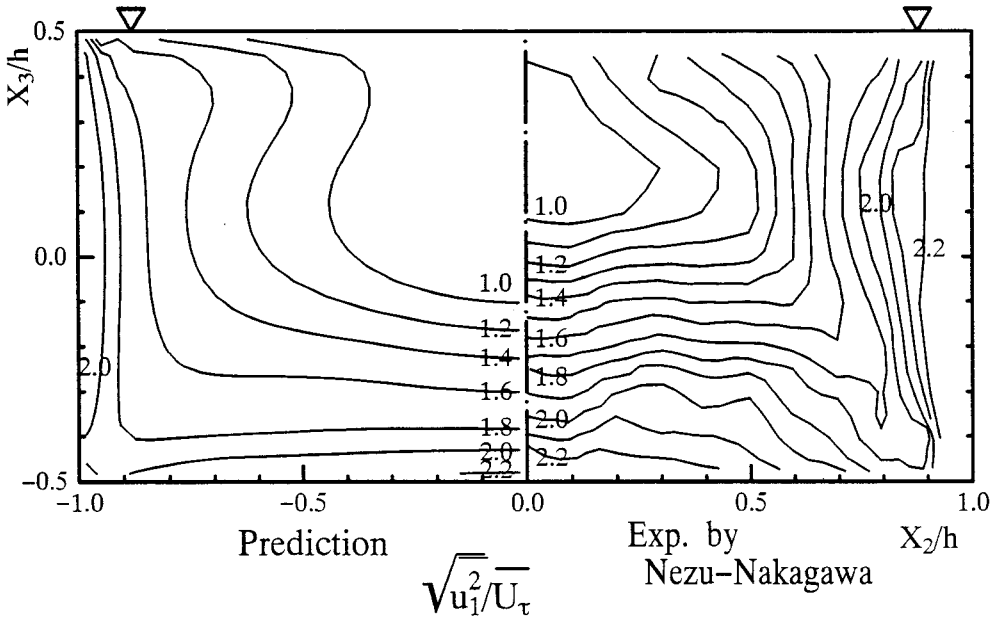

Fig.8: Comparison of $\overline{u_1^2}$ in narrow open channel

In addition to the above examination about mean velocity profiles, distributions of Reynolds stresses are compared with the experiment in order to clarify the validation of the present turbulent model. Figure 8 shows the contour lines for turbulent intensity $\overline{u_1^2}$ of streamwise velocity. Both results are normalized by mean friction velocity $\overline{U_\tau}$ of the bed. In experimental data, relative high value exists near both bed and side wall. The minimum line of this turbulent intensity is below the free surface and it thus corresponds to the velocity-dip phenomenon. The contour map of calculation are similar to that of the experiment except for contour lines near the free surface region. In calculated result, contour lines near the free surface proceed from the channel center toward the side wall. This behavior of contour lines suggests that the turbulent intensity $\overline{u_1^2}$ decays with approaching the free surface. The decrease of $\overline{u_1^2}$ near the free surface coincide with the decrease of turbulent energy k reported experimentally by Nezu

and Nakagawa[18].

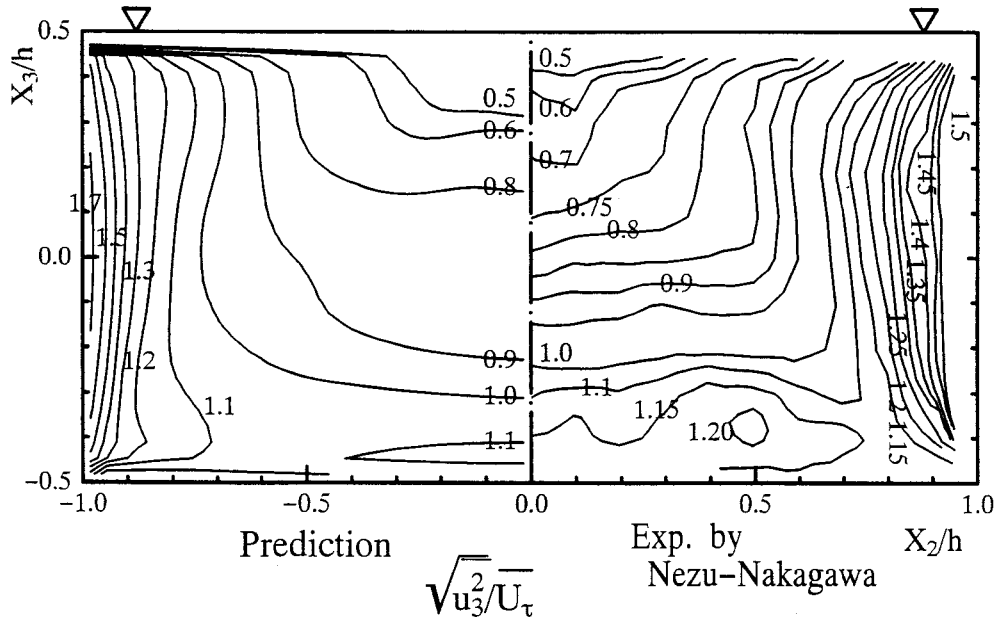

Fig.9: Comparison of $\overline{u_3^2}$ in narrow open channel

Figure 9 shows the contour lines for turbulent intensity $\overline{u_3^2}$ of vertical direction. In the both results, the maximum value of this turbulent intensity exists near the side wall and the minimum value of it exists near the free surface. The vertical intensity decreases monotonously toward the free surface. This decrease of vertical intensity is particularly steep near the free surface. Judging from this damping of vertical intensity, it is easy to guess that the anisotropy of turbulence is strong near the free surface, and consequently a free-surface vortex must be generated.

Moreover, the distribution of shear stress $\overline{u_1 u_3}$ is examined and Fig.10 shows the contour lines for Reynolds shear stress $\overline{u_1 u_3}$. It is found as a characteristic feature that the value of this shear stress is negative in the free surface region in both results. This feature is consistent with the fact that derivative of mean flow U_1 with respect to X_3 is also negative in this region. In comparison with the experimental contours, the calculation forecasts well behavior of contour lines. The fair prediction for the max-line as shown in Fig.3 contribute to this good agreement with the experimental shear stress.

3.2 Numerical Analysis in the Case of Channel Aspect Ratio $B/h = 10$

As described in previous chapter, the velocity-dip phenomenon is one of characteristic features in open channel flow. But Nezu and Nakagawa [4] experimentally found that the velocity-dip phenomenon occurs on condition that B/h is under about 5 or slightly larger. Therefore, open-channel flows can be classified into two categories by the channel aspect ratio B/h. One is

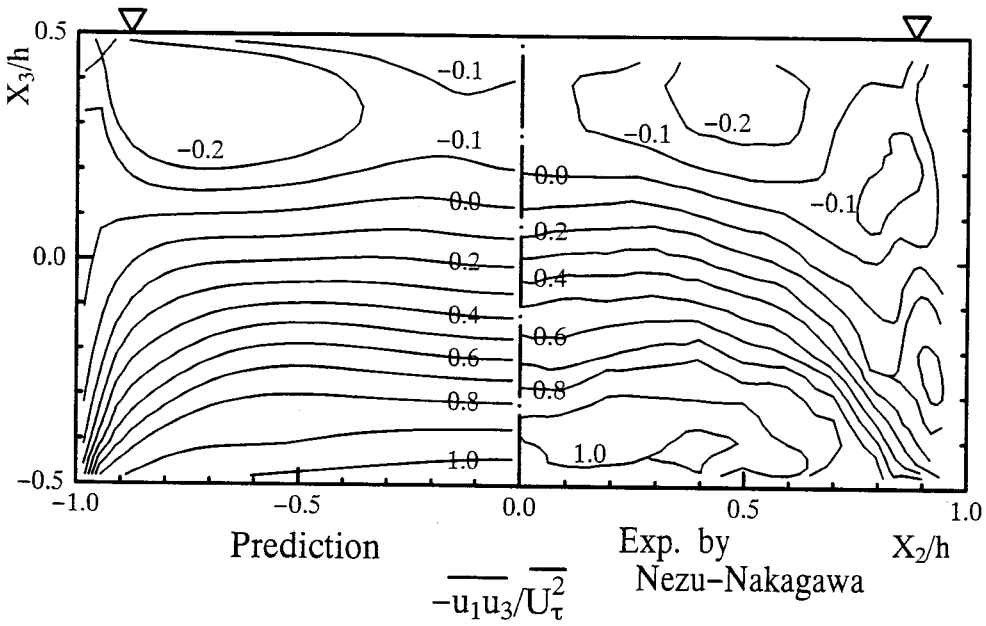

Fig.10: Comparison of $\overline{u_1 u_3}$ in narrow open channel

the narrow open channel characterized by the velocity-dip phenomenon and the other is the wide open channel without velocity-dip phenomenon. To confirm this experimental fact and applicability of the present method to wide open channel flow, numerical analysis has carried out for the fully developed turbulent flow in wide open channel with channel aspect ratio $B/h = 10$.

Figure 11 shows contour lines for the mean streamwise velocity, which are normalized by maximum streamwise velocity. When we draw a line connecting points of local maximum streamwise velocity along the vertical line, max-line is obtained as shown in Fig.11. Comparing with the contour lines displayed in Fig.3, it is clear that the contour lines in wide open channel are different from that in narrow open channel, i.e, the velocity-dip phenomenon is not observed in this wide open channel in both results. On the other hand, as common feature between the narrow and the wide open channel experiment, it is found that distorted contour lines caused by free surface vortex exist near the free surface. Although the calculation is apt to overestimate the experimental results, the calculation reproduces characteristics features in wide open channel flow.

Figure 12 is vector description of secondary current for experiment and numerical results. Although free-surface vortex and bottom vortex are recognized clearly, secondary current does not appear at channel center in both results. As a result of this fact, velocity-dip phenomenon is not recognized in wide open channel flow. Moreover, in comparison with results of narrow open channel, it can be seen that the size of bottom vortex becomes larger than that of bottom vortex in narrow open channel. These results may suggest that the bottom vortex is much

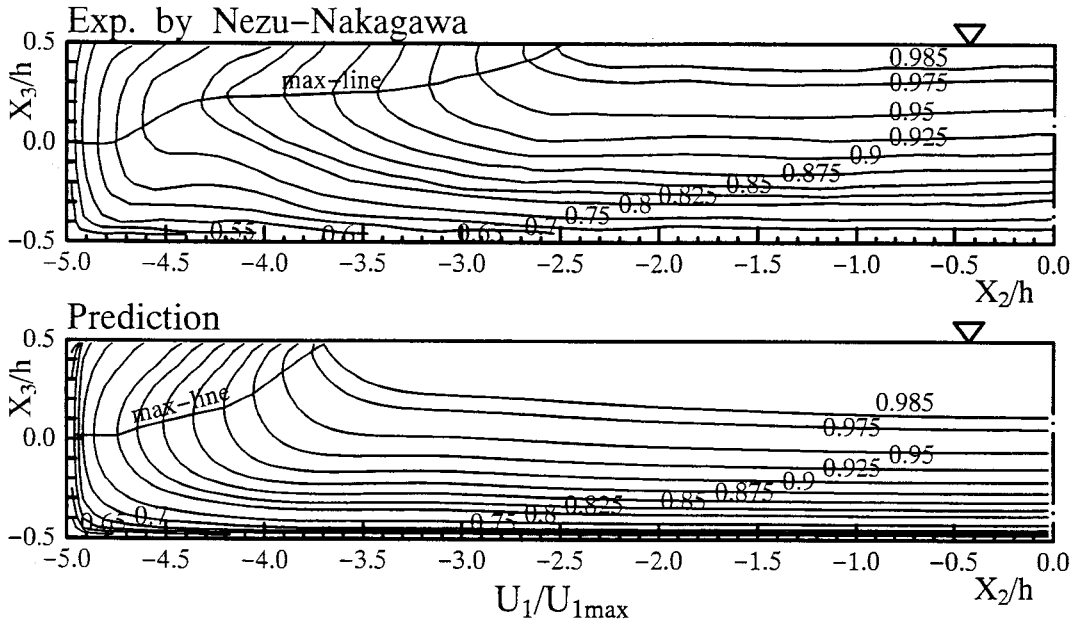

Fig.11: Comparison of streamwise velocity in wide open channel

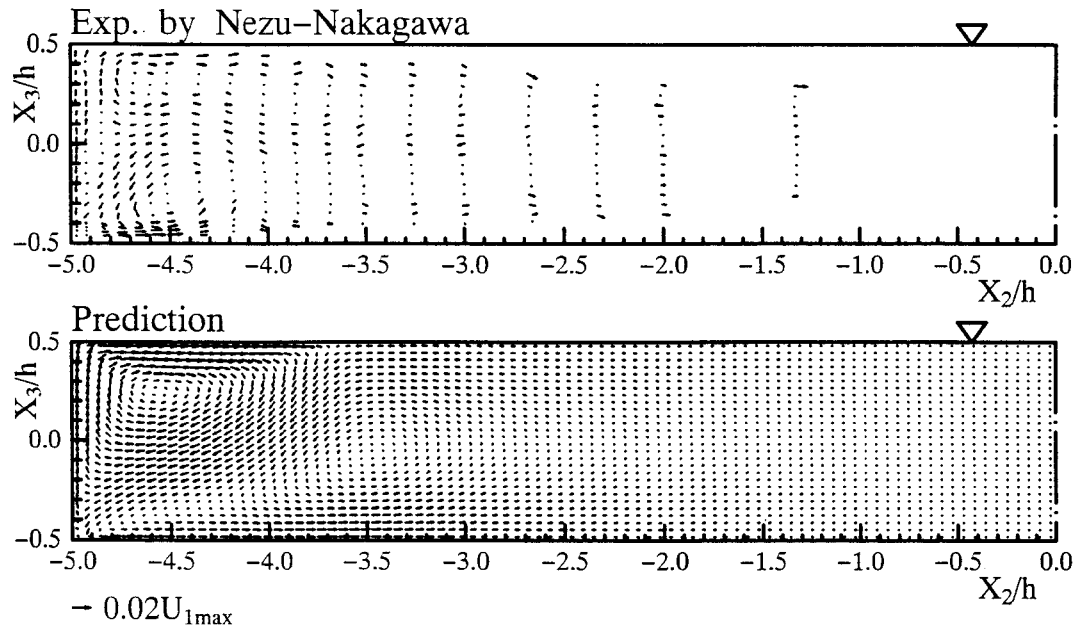

Fig.12: Comparison of secondary currents in wide open channel

affected by the channel aspect ratio and, as channel aspect ratio increases, the size of bottom vortex becomes larger and tends to a constant size.

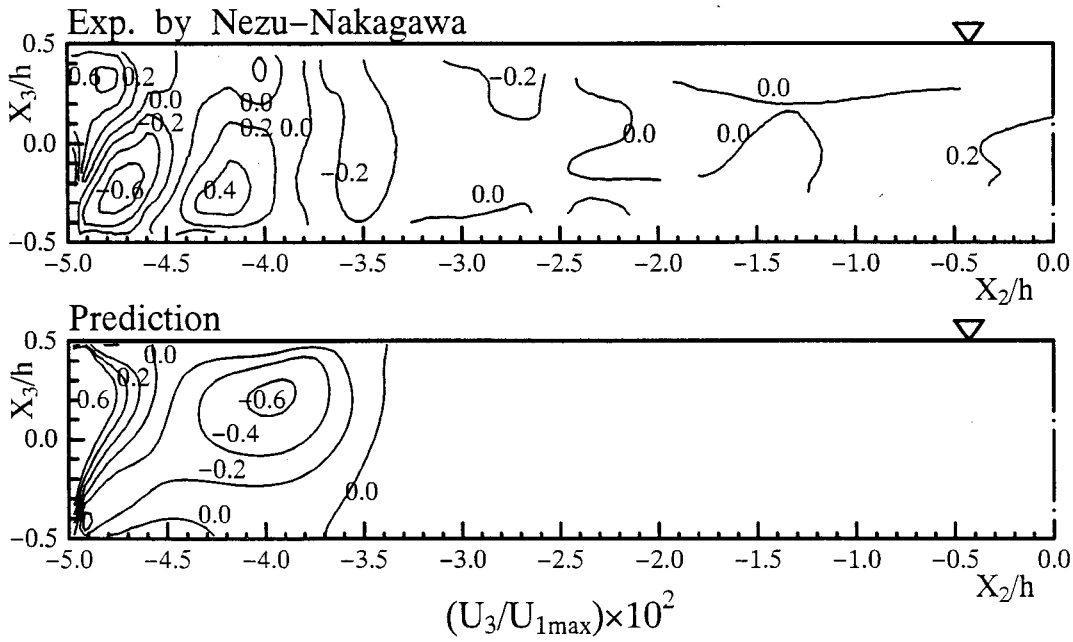

Fig.13: Comparison of vertical velocity in wide open channel

Figure 13 shows contour maps for vertical velocity U_3. In experimental result, the maximum absolute value is located near the side wall and corner region. Although the calculation predict well the value 0.6 near the side wall but does not produce exactly the value -0.6 near the corner region. As the other discrepancy between calculated and experimental results, it is also pointed out that the present method does not forecast the positive value region appeared over $-4.5 < X_2/h < -4.0$.

Figure 14 indicates the distribution of stream line for both results. In calculation, free surface vortex and bottom vortex are clearly recognized from its stream line distribution. In contrast, the experimental stream line shows the existence of counterclockwise vortex lied over between $X_2/h = -3.5$ and -0.5, that is different from the calculated result. The other counterclockwise vortex appeared near the corner region corresponds to big size bottom-vortex of calculation. This discrepancy causes the difference between calculated bed shear stress and experimental one.

Figures 15(a) and (b) show the spanwise distribution of the bed shear stress and side wall respectively, which is evaluated from (8). These shear stress distributions are nondimensionalized by mean shear stress of the corresponding wall. As shown in Fig.15(a), the experimental result indicates mild peak at about $X_2/h = -4.5$ but the calculated result shows it at about $X_3/h = -3.5$. Since appearance of the mild peak is interpreted as a result of the secondary current near the bed changes its flow direction from horizontal direction to upper direction, the

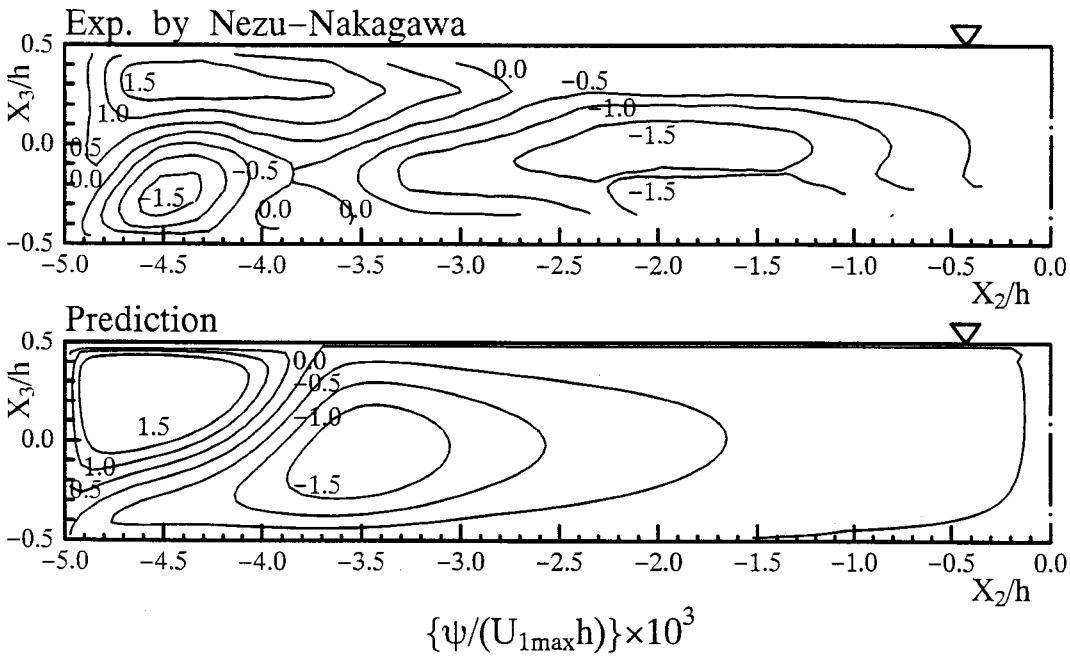

Fig.14: Comparison of streamline in wide open channel

difference of mild peak location coincides with the discrepancy of the size of bottom vortex. As far the shear stress of side wall, its distribution shows the same pattern in narrow open channel flow. It may be said that the shear stress of side wall is not under the influence of channel aspect ratio. The calculated result accords relatively with the experiment.

It is also important to compare the calculated Reynolds stresses with the experiment for the purpose of approving the validity of Reynolds stress model. Turbulent intensity of streamwise velocity normalized by mean friction velocity of the bed is presented in contoured form in Fig.16. By transporting high momentum fluid toward the corners, it causes a bulging of the velocity contours toward the corners. This bulging of contour lines are clearly observed in the experimental data near the corner region, while in the case of calculation, they are not recognized so clear as the experiment. This fact suggests that the intensity of the bottom vortex is not so strong than that of the experiment. Moreover, the great discrepancy between the calculation and the experiment is behavior of contour lines near the free surface. In calculated result, contour lines near the free surface proceed from the channel center toward the side wall as well as in the case of narrow open channel. This behavior of contour lines indicates that the turbulent intensity $\overline{u_1^2}$ decays with approaching the free surface.

The calculated result of turbulent intensity $\overline{u_3^2}$ of vertical direction illustrates in Fig.17, in parallel with corresponding experiment. In comparison with the experiment, the calculation forecasts the value of near bed and side walls. As common characteristic feature between the calculation and the experiment, it is proposed that the vertical intensity decreases monotonously from the bed toward the free surface and rapid decrease of vertical intensity exists extremely

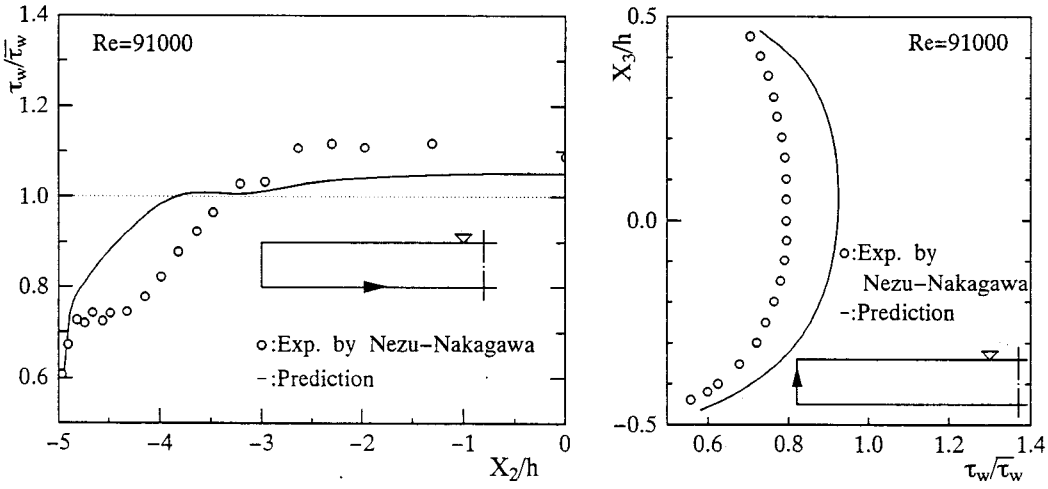

(a) Shear stress along bed (b) Shear stress along side wall

Fig.15: Comparison of wall shear stress in wide open channel

near the free surface. Open channel flow is characterized by this rapid decrease of vertical intensity regardless of channel aspect ratio.

Contour maps of shear stress $\overline{u_1 u_3}$ are presented in Fig.18. In the light of shear stress pattern in narrow open channel as shown in Fig.10, contour lines in wide open channel flow are similar in point of existence for negative and positive regions divided by the zero line. The present method can predict the pattern of zero line and the value near the bed without great discrepancy with the experiment.

3.3 Origin of Secondary Currents

The measurement described above have shown the magnitude and effects of the secondary motion, but they give no indication as to its origin. In the following, the vorticity balance is examined in a narrow and wide open channels by evaluating the several terms in the vorticity transport equation using the calculated results in order to make the mechanism for generation of free surface vortex and bottom vortex clear. For a steady incompressible constant-property and a fully developed turbulent flow, the vorticity transport equation for streamwise vorticity is expressed as follows (in the coordinate system given in Fig.1):

$$U_2\frac{\partial \omega_1}{\partial X_2}+U_3\frac{\partial \omega_1}{\partial X_3}=\frac{\partial^2}{\partial X_2 \partial X_3}\left(\overline{u_2^2}-\overline{u_3^2}\right)+\left(\frac{\partial^2}{\partial X_3^2}-\frac{\partial^2}{\partial X_2^2}\right)\overline{u_2 u_3} +\nu\left(\frac{\partial^2 \omega_1}{\partial X_2^2}+\frac{\partial^2 \omega_1}{\partial X_3^2}\right) \tag{9}$$

where the components of the vorticity vector are:

$$\omega_1=\frac{\partial U_3}{\partial X_2}-\frac{\partial U_2}{\partial X_3}. \tag{10}$$

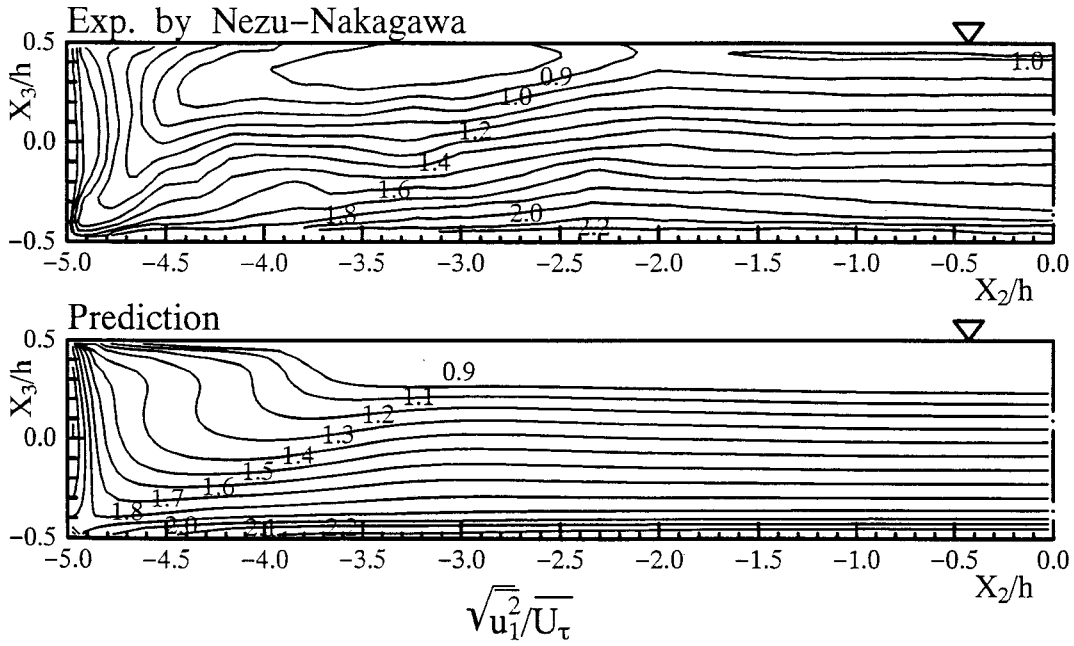

Fig.16: Comparison of $\overline{u_1^2}$ in wide open channel

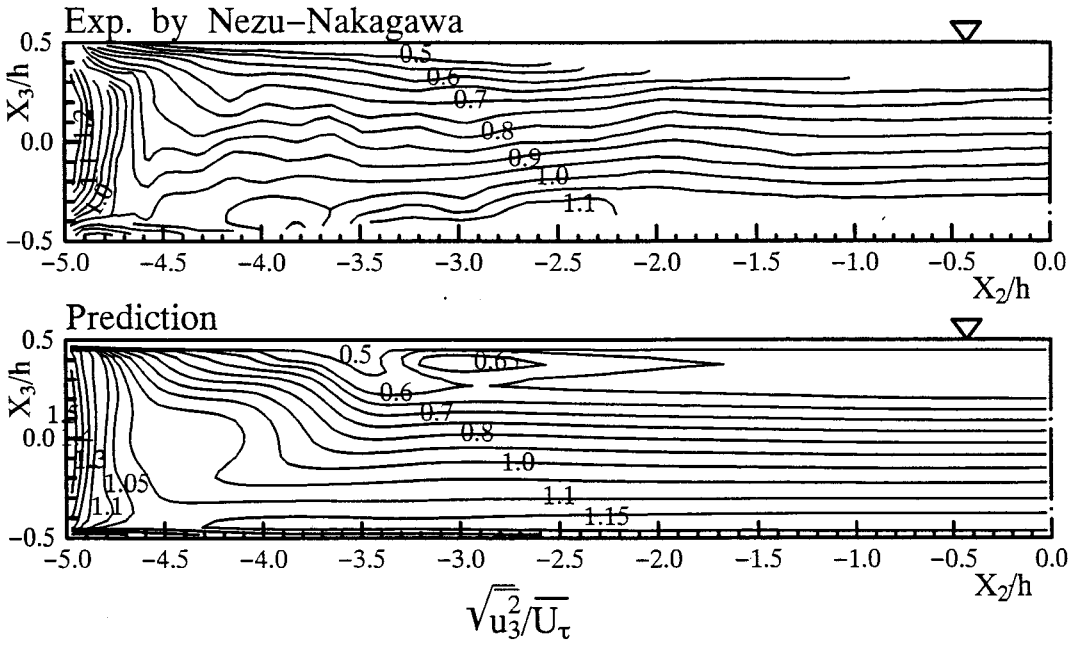

Fig.17: Comparison of $\overline{u_3^2}$ in wide open channel

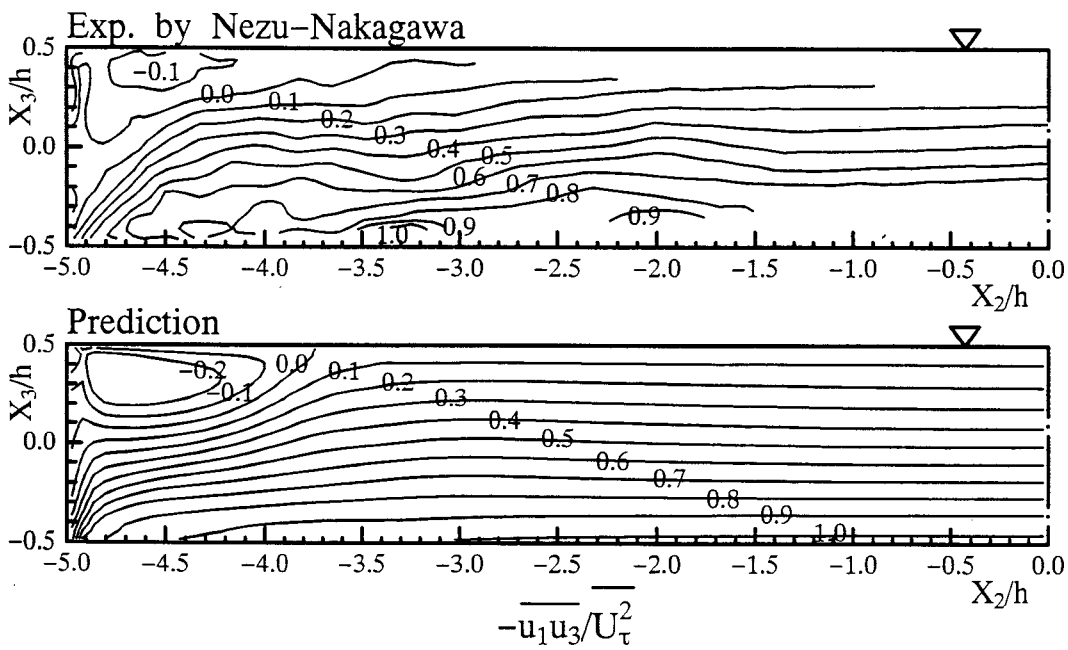

Fig.18: Comparison of $\overline{u_1 u_3}$ in wide open channel

In the above equation of fully developed flow, the first and second terms of left hand side represent convection of vorticity by the mean flow, and the first and second terms of right hand side express the influence of the turbulent stresses on the production or destruction of streamwise vorticity, and the third term the damping by viscosity. The secondary flow of the second kind is caused by anisotropy of turbulent stresses,i.e, by the contributions of the first, second terms on the right hand side of (9). The distributions of these production terms are evaluated in narrow and wide open channel by using calculated results. These distributions of narrow and wide open channel are shown in Figs.19(a) and 19(b), respectively.

In the case of narrow open channel, the maximum absolute value appears near the free surface of side wall. Therefore, this calculated result indicates that anisotropic turbulence near the free surface of side wall plays a major role in the generation of the free surface vortex. On the other hand, judging from the relative high value is recognized near the corner region, bottom vortex is generated by the anisotropic turbulence near the corner region. Since the value of production term near the free surface is much greater than that of production near the corner region, the free surface vortex becomes larger and stronger, depressing the bottom vortex to the bed. As for the distribution of production terms in wide open channel flow, the maximum absolute value exists near the free surface of the side wall as well as in the case of narrow open channel but its value is not larger than that of narrow channel. From estimation of the production terms for vorticity equation by making use of calculated results, it can suggest that the free surface vortex is generated mainly near the free surface of the side wall regardless of channel aspect ratio by the non-homogeneity and anisotropy of turbulence, which are induced by the decrease of vertical velocity fluctuation approaching the free surface.

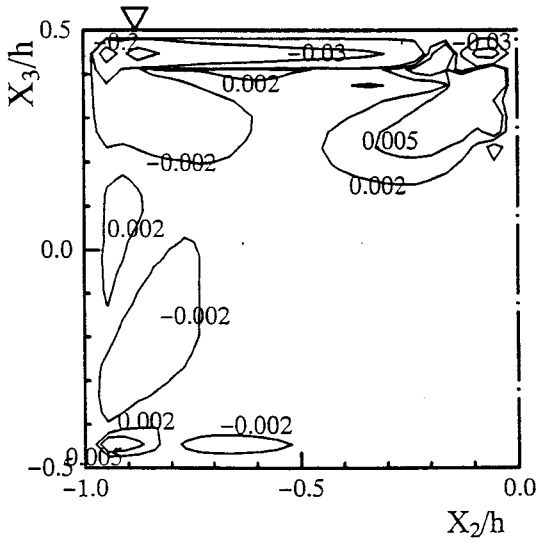

(a) Narrow open channel

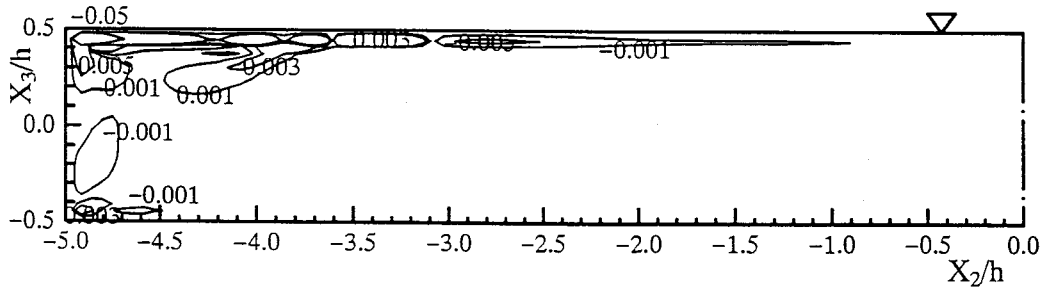

(b) Wide open channel

Fig.19: Production terms fro streamwise vorticity

3.4 Developing behavior of secondary currents

Numerical analysis has been carried out for developing turbulent flow in narrow open channel flow with channel aspect ratio $B/h = 2$. To our knowledge, detailed and reliable results for the developing behavior of the secondary currents in open channel flow have not been reported previously. Therefore, it is important and profitable for river engineers to make developing behavior of secondary currents clear. The velocity vectors of secondary current and the contour lines of streamwise velocity at typical locations are shown in Fig.20.

At location $X_1/4R = 4.84$ from the inlet of open channel, the free surface vortex is evidently recognized near the free surface of side wall with great intensity and bottom vortex also exists near the corner region. Moreover, it can be seen as a characteristic feature that the place of the maximum value for streamwise velocity coincides with that of the maximum intensity of secondary currents as shown in the contour lines of streamwise velocity. As the flow develops, the size of free surface and bottom vortices becomes gradually great as shown in the results

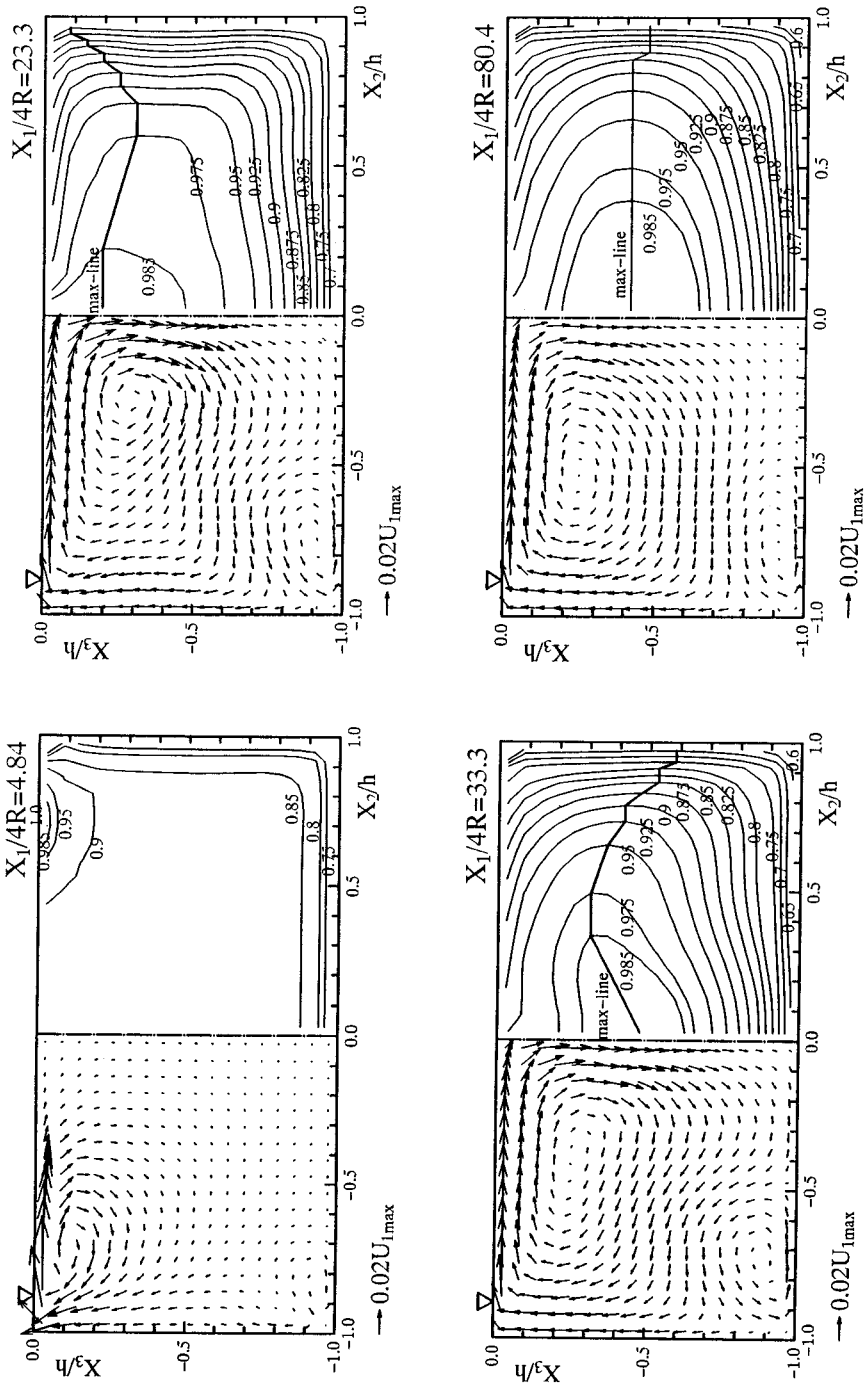

Fig.20: Developing behavior of secondary currents

of further downstream. The calculated results at $X_1/4R = 23.3$ verified that the velocity-dip phenomenon is already recognized at this location. Furthermore, calculated results at $X_1/4R = 33.3$ shows a dramatic alteration in the pattern of streamwise velocity, i.e, the maximum value of streamwise velocity appears further downward location than that of a fully developed turbulent flow at $X_1/4R = 80.4$. After this characteristic appearance of velocity-dip, the intensity of secondary currents reaches constant value with decaying its intensity as the flow develops further downstream. These calculated results of developing turbulent flow suggests that the intensity of secondary flow increases gradually as the flow develops and reaches to the maximum value at about $X_1/4R = 33.3$ and, after this appearance of maximum value, its intensity decays with approaching the constant value. In addition, calculated results indicate that the maximum streamwise velocity of the cross section exists at further location from the free surface than that of maximum streamwise velocity for a fully developed turbulent flow on the way of developing turbulent flow.

4.CONCLUSIONS

Numerical analysis has been carried out for developing turbulent flow in open channel with channel aspect ratio $B/h = 2$ and for developing turbulent flow with channel aspect ratio $B/h = 10$. In order to predict preciously anisotropy turbulence, algebraic Reynolds stress model is adopted,i.e, the convection and diffusion terms are transformed from differential equation into algebraic equation. Moreover, of major importance is the boundary condition at the free surface. In this research, the boundary condition is presented newly. The calculated results are compared with the experimental data available.

In comparison with the experimental results, the present method can predict well the characteristic features in open channel flow. For example, the velocity-dip phenomenon and the monotonous increase of bed shear stress toward the channel center are forecasted well in narrow open channel by the present method. Adding to this, it is reported experimentally that the velocity- dip phenomenon is not observed in the case of the wide open channel flow. The present calculation also predict this disappearance of the velocity-dip phenomenon in wide open channel flow. Judging from the comparison with the experimental results, it is confirmed that the present Reynolds stress model and the boundary condition at the free surface is applicable to the open channel flow regardless of channel aspect ratio. Furthermore, as for the developing turbulent flow in narrow open channel flow, calculated results of secondary currents and streamwise velocity suggests that the intensity of free surface vortex shows its the maximum value at midway between the inlet and outlet section,i.e.,its maximum value exists before reaching a fully developed flow. As a result of this appearance, the maximum streamwise velocity of the cross section is located further downward from the free surface than the location of maximum streamwise velocity for the fully developed turbulent flow region.

Acknowledgments

The authors would like to express their thanks to Prof. I. Nezu and Prof. H. Nakagawa, Kyoto University, who kindly allowed us to use their experimental results in this paper and also provide us valuable suggestions and discussions on this numerical analysis.

REFERENCES

[1] N.Rajaratnam and D. Muralidhar (1969) Boundary shear stress distribution in rectangular open channels; La Houille Blanche, vol.6 pp.603-609

[2] W.D.Knight, J.D.Demetriou and M.E.Hamed (1984) Boundary shear in smooth rectangular channels; J. Hydraulic Eng., ASCE, vol.110 pp.405-422

[3] H.Nakagawa, I.Nezu and H.Ueda (1975) Turbulence of open channel flow over smooth and rough beds; Proc.of Japan Soc. Civil Engrs., vol.241 pp.155-168

[4] I.Nezu and H.Nakagawa (1985) Three-dimensional turbulent structure in open channel flow and effect of free surface on its structure; Annuals of Disaster Prevention Research Institute, Kyoto University, (in Japanese) vol.28 pp.499-522

[5] H.A.Einstein and H.Li (1958) Secondary currents in straight channel; Trans. Amer. Geophys. Union, vol.39 pp.1085-1088

[6] D.Naot and W.Rodi (1982) Calculation of secondary currents in channel flow; J. Hydraulic Eng., ASCE, vol.108 No.HY8 pp.948-973

[7] I.Nezu and H.Nakagawa (1987) Numerical calculation of turbulent open channel flows in consideration of free-surface effect; Memoirs, Fac. of Eng., Kyoto University, vol.49 No.2 pp.111-145

[8] I.Celik and W.Rodi (1984) Simulation of free-surface in turbulent channel flows; Physicochemical Hydrodynamics, vol.5 pp.217-227

[9] D.Naot, I.Nezu and H. Nakagawa (1992) Numerical calculation of three-dimensional turbulent flow in compound rectangular open channels; Memoirs, Fac. of Eng., Kyoto University, vol.54 No.2 pp.49–82

[10] W.Rodi (1976) A new algebraic relation for calculating the Reynolds stresses; Z. Angew. Math. Mech., vol.56 pp.T219-T221

[11] P.Y.Chou (1945) On velocity correlations and the solutions of the equations of turbulent fluctuation; Quart. Appl. Math., vol.3 pp.38-54.

[12] B.E.Launder, G.J.Reece and W.Rodi (1975) Progress in the development of a Reynolds stress turbulence closure; J. Fluid Mech., vol.68 pp.537-566

[13] H.Sugiyama, M.Akiyama, M.Matsumoto, M.Hirata and N.Ninomiya (1993) Numerical analysis of fully developed turbulent flow in a square duct with two facing roughened walls; C.F.D. Journal, vol.2 no.3 pp.319-338

[14] F.H.Champagne, V.G.Harris and S.Corrsin (1970) Experiments on nearly homogeneous turbulent shear flow; J. Fluid Mech., vol.41 pp.81-139

[15] V.G.Harris, J.A.H.Graham and S.Corrsin (1977) Further experiments in nearly homogeneous turbulent shear flow; J. Fluid Mech., vol.81 pp.657-687

[16] J.C.R.Hunt (1984) Turbulent structure and turbulent diffusion near gas-liquid interfaces; *Gas transfer at water surfaces*, Reidel Pub., pp.67-82

[17] D.Naot and W.Rodi (1982) Calculation of secondary currents in channel flow; J. Hydraulics Div., ASCE, vol.108 pp.948-968

[18] I.Nezu and H.Nakagawa (1987) Numerical calculation of turbulent open-channel flows by using a modified $k-\varepsilon$ turbulence model; Proc. of Japan Soc. Civil Engrs., (in Japanese) vol.387 pp.125-134

[19] M.M.Gibson and W.Rodi (1989) Simulation of free surface effects on turbulence with a Reynolds stress model; J. Hydraulic Research, IAHR., vol.27 pp.233-244

[20] D.Naot, I.Nezu and H.Nakagawa (1993) Free surface renewal and the modeling of turbulent structure in compound open-channel flow; Ninth Symp. on Turbulent Shear Flows, pp.26/3/1-26/3/6